ELSEVIER

Thermochimica Acta 369 (2001) 95–116

thermochimica acta

www.elsevier.com/locate/tca

Phenomenological study of enthalpy relaxation of amorphous glucose, fructose, and their mixture

Ratchapong Wungtanagorn[a,1], Shelly J. Schmidt[b,*]

[a]*Department of Agricultural Engineering, University of Illinois at Urbana-Champaign, 367 Bevier Hall, 905 South Goodwin Avenue, Urbana, IL 61801, USA*

[b]*Department of Food Science and Human Nutrition, University of Illinois at Urbana-Champaign, 367 Bevier Hall, 905 South Goodwin Avenue, Urbana, IL 61801, USA*

Received 18 May 2000; received in revised form 12 October 2000; accepted 16 October 2000

Abstract

Enthalpy relaxation of glucose, fructose, and their mixtures (75/25, 50/50, and 25/75 glucose/fructose) has been investigated in terms of the Tool–Narayanaswamy–Monihan (TNM) and the Adam–Gibbs model parameters using differential scanning calorimetry (DSC) data. The apparent activation energy was evaluated from the cooling rate dependence of the limiting fictive temperature and was found to decrease as the fructose content increased. The non-linear parameter x and the exponential parameter β obtained from the TNM model was found to be the same as those obtained from the Adam–Gibbs model within their standard deviations. The value of parameter x increased from 0.50 in glucose to 0.75 in fructose, while parameter β decreased from 0.64 in pure glucose to 0.50 in the 50% fructose mixture and remained at about 0.50 for the mixtures with over 50% fructose content. The parameter x which reflects the relative contributions of the temperature and structure dependence of the relaxation times was also evaluated using the peak-shift method. The values of parameter x obtained from the peak-shift method for all sugars were found in general to be higher than those obtained from curve fitting to the TNM and the Adam–Gibbs models. The fragility of the sugars was also evaluated using the enthalpy relaxation data. The addition of fructose to the glucose–fructose system produced ''stronger'' liquids, and less non-linear behavior.

Keywords: Physical aging; DSC; Glucose; Fructose; Enthalpy relaxation

1. Introduction

Structural relaxation refers to the time-dependent change of any macroscopic property (volume, enthalpy, refraction index, electrical conductivity or viscosity) of the liquid following a perturbation (i.e. a change in temperature or pressure) [1]. When a liquid is subject to a rapid change in temperature, the macroscopic properties of the liquid exhibit an instantaneous change, followed by a slower structural relaxation to a new equilibrium property value at the new temperature [2]. Microscopically, the structural relaxation process is considered to correspond to the kinetically impeded rearrangement of the temperature-dependent structure of the liquid [1]. The liquid becomes a rigid glass, when the time required for structural change is much longer than the time of observation and within the given experimental time scale the glass can no

* Corresponding author. Tel.: +1-217-333-1324; fax: +1-217-244-7877.
E-mail addresses: wungtana@uiuc.edu (R. Wungtanagorn), sjs@uiuc.edu (S.J. Schmidt).
[1] Tel.: +1-217-333-3196.

0040-6031/01/$ – see front matter
PII: S0040-6031(00)00741-3

longer achieve structural equilibrium [3]. Therefore, structural relaxation, as often observed within and somewhat below the glass transition region, is a result of the non-equilibrium nature of the glassy state. Structural relaxation reflects the spontaneous approach of the material towards equilibrium at a rate that depends on the temperature, and the complete thermal history of the glass [4]. In particular, the isothermal structural relaxation that occurs below glass transition temperature (T_g) is often referred to as physical aging [5].

Many processes used in the preparation of food products such as dehydration, concentration, extrusion, or melting transform the crystalline sugar components into amorphous sugars. The amorphous sugars in sugar containing products, such as hard candy and low moisture foods, are in a metastable, non-equilibrium state and can be subject to physical aging during their shelf life. The role of physical aging in food materials is that it may produce unfavorable changes in some physical properties (density, hardness and brittleness), which in turn affect the quality and stability of the food products. As pointed out by Roos [6], information on structural relaxation that reflects the physical state of amorphous foods would probably be useful in evaluation the brittleness or cracking behavior of glassy foods and food components.

Structural relaxation has been studied intensively in polymers by dilatormetry (volume relaxation, [7]) and differential scanning calorimetry (DSC) (enthalpy relaxation, [8]). In the present paper, the structural relaxation of two commonly used sugars (glucose, fructose) and their mixtures has been investigated using DSC. The characterization of the relaxation process was evaluated through the kinetic parameters of the TNM (Tool, Narayanaswamy, and Moynihan) and Adam–Gibbs models. Although, the kinetic parameters have been evaluated and reported for various non-foods, materials such as PVC, PMMA, and PS [9–11], only a few studies have been conducted on food materials [12–14]. The objectives of this research are: (1) to evaluate the enthalpy relaxation of glucose, fructose, and their mixtures through the kinetic parameters TNM and Adam–Gibbs models obtained from the curve-fitting method, (2) to compare the non-linearity parameter x obtained from the curve-fitting method and the peak-shift method, and (3) to classify glucose and fructose into the strong/fragile classification of Angel [15].

2. Phenomenolgical expressions of the models

It is well established that enthalpy relaxation is both non-exponential and non-linear. The non-exponential character of the enthalpy relaxation is treated by taking a distribution of relaxation times into account and is frequently described using the Kohlrausch–Williams–Watts (KWW) stretched exponential function. The KWW function is generalized for the non-linear case as shown in Eq. (1) [16–18]:

$$\phi(t) = f(t, \tau_0) = \exp(-\zeta^{\beta}) = \exp\left(-\left(\int_0^t \frac{\mathrm{d}t}{\tau_0(t)}\right)^{\beta}\right) \tag{1}$$

where $\phi(t)$ is the relaxation function, ζ the reduced time, τ_0 represents the characteristic relaxation time which is a function of time (t), β is a parameter characterizing the width of the relaxation time distribution spectrum ($0 \leq \beta \leq 1$).

In most models, the non-linear character of the enthalpy relaxation is taken into account based on the concept of Tool [19] in that the relaxation times (τ_0) are considered to depend on both temperature and the average structural state of the system. The fictive temperature (T_f) was introduced in order to characterize the structural state of the system. T_f was defined as the temperature at which an intensive property in an equilibrium sample would have the same value as that exhibited by the glass in question. It should be mentioned that T_f varies significantly depending on which intensive property is selected as the reference. The concept of Tool was further developed by Narayanaswamy and coworkers [17,18] and Moynihan [20] and is given as the TNM (Tool, Narayanaswamy, and Moynihan) model in Eq. (2):

$$\tau_0(T_a, T_f) = A \exp\left[\frac{x\,\Delta h^*}{RT_a} + \frac{(1-x)\,\Delta h^*}{RT_f(t)}\right] \tag{2}$$

where A is the relaxation time in equilibrium at an infinitely high temperature, Δh^* the apparent activation energy (a constant) in the equilibrium state above T_g, $x\,\Delta h^*$ denotes the activation energy in the glassy state at a fixed value of $T_f = T_f'$ [10], R represents the

ideal gas constant, T_a the aging temperature, and x ($1 \geq x > 0$) denotes the non-linearity parameter that determines the boundaries of the degree of non-linearity or partitions the effects of T and T_f. Physical aging is described in terms of the isothermal time dependence of T_f. The difference between T_f and T, therefore, defines the departure of the aged system from equilibrium.

Another expression of τ_0 was proposed by Scherer [21,22] who first used the Adam–Gibbs theory explicitly for enthalpy relaxation. This concept was further refined by Hodge [9,23], who proposed the present form of the model, referred to as Adam–Gibbs–Fulcher (AGF) shown in Eq. (3):

$$\tau_0(T, T_f) = B \exp\left(\frac{Q}{RT(1 - (T_2/T_f))}\right) \quad (3)$$

where B and Q are constants, and T_2 denotes the temperature at which the configurational entropy of the equilibrium liquid would vanish. T_2 was found to be equivalent to the Kauzmann temperature T_K in some polymers [10]. The parameters of both the TNM and Adam–Gibbs models can be obtained by curve fitting the experimental heat capacity data.

Another way to obtain the non-linearity parameter x is called the peak-shift method which was originally based on the Kovacs–Alkonis–Hutchinson–Ramos (KARH) model [24]. The peak-shift method evaluates the parameter x based on the endothermic response of a glass on heating to a given thermal and aging history [25–29]. Three well-defined thermal cycles are used in the method: (i) cooling at a constant rate (q_c) from equilibrium at T_0 to an aging temperature T_a below T_g; (ii) isothermal aging at T_a, which results in a decrease in the enthalpy by an amount δ_H; and (iii) reheating at a constant rate, q_h, until equilibrium is again achieved. During the heating scan, the specific heat capacity passes through a maximum at a peak temperature (T_p) which is dependent on four experimental parameters: cooling rate (q_c), aging temperature (T_a), enthalpy loss (δ_H), and heating rate q_h. When the sample is aged for a long period of time (fully stabilized), the dependency of T_p on these experimental parameters can be expressed in terms of a set of shifts $\hat{s}$. For example, $\hat{s}(Q_h)$ is the heating rate dependent shift. The shifts were found to be interrelated and critically dependent on the non-linearity parameter x, but were not dependent upon the shape and width of the relaxation distribution spectrum, when the glass was conditioned to the well-defined thermal and aging history described above [27,28]. The peak-shift method has been applied successfully in polymeric and inorganic glasses to determine the non-linear parameter x [30–38].

The "strong/fragile" classification proposed by Angell and coworkers [15,39–45] is used to describe the temperature dependence of the relaxation properties in the equilibrium state. The interpretation of the glassy state relaxation (non-equilibrium) behavior within this classification has been attempted in structural relaxation studies for a variety of materials such as, polyvinylchloride, polystyrene, polymethylmethacrylate, and polycarbonate [9,10,25,34,38,46–50].

3. Materials and methods

3.1. Materials, sample preparation, and instrumentation

D-(−)-Fructose (D-Levulose) (Product no. G-2543, SigmaUltra grade) and anhydrous D-(+)-glucose (Product no. G-7528, SigmaUltra grade) were obtained from Sigma (St. Louis, MO) and used without further purification. Both sugars were screened with 3 in. stainless frame and cloth sieves (W.S. Tyler, Mentor, OH) and only particle sizes between 0.180 (No. 80) and 0.212 (No. 70) micrometers were collected. After screening, the sugars were dried in a vacuum oven at 60°C and 14.7 psi for 12 h. Three weight ratios of dry glucose to fructose, 75/25, 50/50, and 25/75 (denoted as G75F25, G50F50, and G25F75, respectively) were prepared. Hermetic uncoated aluminum pans and lids were used in all experiments and were cleaned in acetone before use. All samples (10 mg ± 0.1 mg) experienced the entire thermal history in the DSC cell, including the aging step. All experiments were done in duplicate.

A TA Instrument 2920 MDSC, equipped with a refrigerated cooling accessory, Universal Analysis software, and Thermal Analysis-Heat Capacity software, was used. Dry helium gas was used as the purge through the sample cell at a rate of 25 cm^3/min. Dry nitrogen gas was used to purge the refrigerated cooling accessory during heating, whereas dry helium gas was used during cooling in order to achieve the highest

efficiency of cooling. The flow rate of both gases was at a rate of 150 cm^3/min.

Indium and sapphire were used for cell constant and temperature calibration, and heat capacity calibration, respectively. An empty aluminum DSC pan was used as the reference pan and matched to within ±0.05 mg in weight of the empty sample pan. Heat capacity data were obtained using the Heat Capacity Analysis software [51]. The values of the midpoint T_g of the unaged glucose, 75G25F, 50G50F, 25G75F, and fructose determined at equal cooling–heating rate of 10 K/min using the Universal Analysis software [52] were 310.07 ± 1.188, 299.67 ± 0.028, 290.83 ± 0.544, 284.69 ± 0.559, and 278.30 ± 0.248 K, respectively.

3.2. Thermal history

A schematic illustration of the entire thermal history applied to all samples is shown in Fig. 1. For all samples, the sugar crystals were initially melted in the DSC pan by heating from ambient temperature to 441.2 K at 10 K/min and held for 0.3 min in order to completely melt the sugar crystals. The thermal histories for each experiment are described below.

3.2.1. Unaged experiments

The molten sugar was cooled at a cooling rate q_c to T_l, about 55 K below its T_g midpoint (T_l = 256.2, 244.7, 238.2, 233.2, 226.2 K for glucose, 75G25F, 50G50F, 25G75F, and fructose, respectively) in order to form an amorphous glass (path ABO). The sample was then reheated to 393.2 K at a heating rate q_h (path OCA). The cooling rate q_c and heating rate q_h are specified later in each corresponding section.

3.2.2. Aging experiments

The molten sugar was cooled (path AB) at a cooling rate of 10 K/min and aged at a temperature T_a about

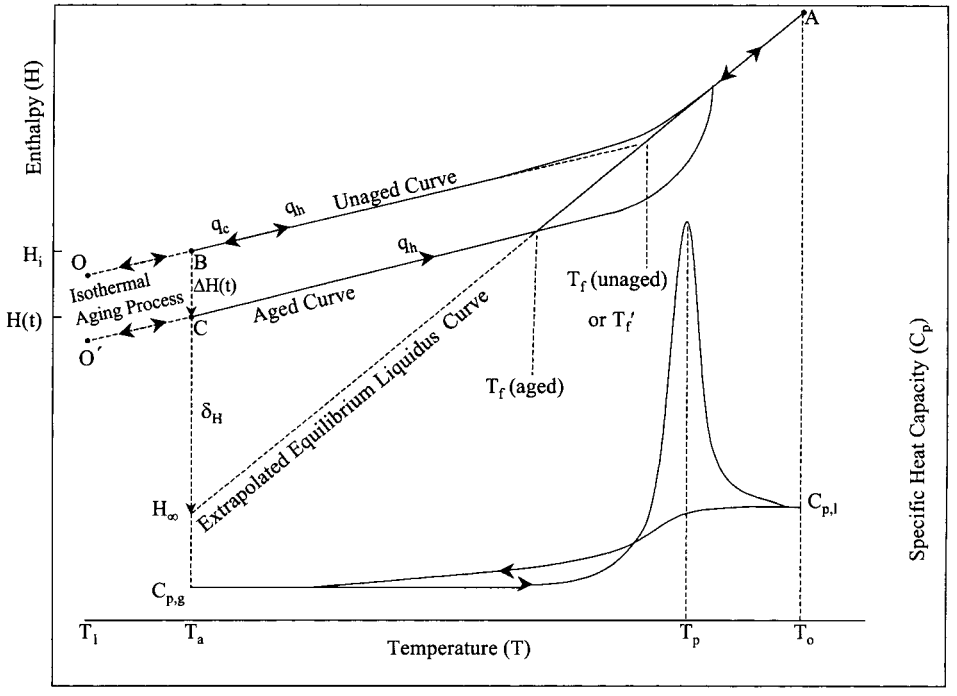

Fig. 1. Schematic diagram of the change in enthalpy and specific heat capacity of glucose, fructose, and their mixtures with isothermal aging at T_a (path ABCO′CA) and without aging (path ABOBA). The samples were cooled at a cooling rate q_c and heated at a heating rate q_h. H_i and H_t are the enthalpies at the beginning of aging and at aging for time t, respectively. The equilibrium enthalpy at aging temperature T_a is H_∞. $C_{p,l}$ is the specific heat capacity of the equilibrium liquid and $C_{p,g}$ is that of the glass. T_f (unaged) and T_f (aged) are the fictive temperatures of unaged and aged samples, respectively. $\Delta H_t = H_i - H_t$ and $\delta H = H_t - H_\infty$, respectively. T_p denotes the maximum peak of the heat capacity curve during reheating scan through the glass transition region.

10 K below the T_g midpoint (path BC). The aging temperatures (T_a) of glucose, 75G25F, 50G50F, 25G75F, and fructose are 301.2, 289.7, 282.7, 277.7, and 271.2 K, respectively. An additional aging temperature of 272.7 K was also used for the 50G50F sample. The aging time (t_a) varied from 5 min to 7 days. As a result of aging, the enthalpy of the sample decreases from H_i to $H(t)$ (path BC). After aging, the sample was cooled at 10 K/min to T_1 (path CO′) and then reheated at 10 K/min to 393.2 K.

3.2.3. Peak-shift experiment

The molten sugar was cooled at a cooling rate (path AB) of 10 K/min and aged at T_a (see aging experiment) for 720 min in all samples (path BC). After aging, the sample was cooled at 10 K/min to a temperature of 281.2, 269.7, 262.7, 257.7, and 251.2 for glucose, 75G25F, 50G50F, 25G75F, and fructose, respectively (about 30 K below its T_g midpoint, path CO′, instead of 55 K in order to minimize the aging effect during cooling from T_a to T_1). This step was slightly changed from the original thermal history described by Hutchinson and Rudy [26] for the peak-shift method in that the sample was reheated to T_0 immediately after aging without cooling down to T_1. However, the conditions used in this research were similar to that used by Godard et al. [53] for 2-poly[methyl(α-*n*-alkyl)acrylates]. The process of cooling the sample from T_a to T_1 will be considered to have no appreciable effect on the relaxation process [54]. The sample was then reheated to obtain the position of the peak temperature (T_p) at five heating rates of 2.5, 5, 10, 15 and 20 K/min to 393.2 K. These T_p values are used in Section 4.4.

3.3. Calculation and optimization procedures for the TNM and Adam–Gibbs models

At temperatures well below and well above the glass transition, the heat capacity data was assumed to be independent of time and was well approximated by a linear function of temperature, i.e. heat capacity in the glass state: $C_{p,g}(T) = a + bT$ and heat capacity in the liquid state: $C_{p,l} = A + BT$, where a, b, A, and B are constants obtained from the linear least squares fitting to the linear regions of glass and liquid heat capacities. T_f was determined by measuring the change in enthalpy as it is heated through the transition region and was defined in terms of the heat capacity as [2,20]:

$$\int_{T_f}^{T^*} (C_{p,l} - C_{p,g})\,dT' = \int_{T}^{T^*} (C_p - C_{p,g})\,dT' \qquad (4)$$

where C_p is the observed heat capacity, T' denotes a dummy variable, and T^* a reference temperature well above the glass transition region where the system is in equilibrium at the heating or cooling rate of interest. Experimental $C_p(T)$ data were normalized with respect to the difference between the liquid and glass heat capacities using the procedure developed by Moynihan and coworkers [2,20]. The normalized heat capacity, C_p^N, is defined as the temperature derivative of T_f at temperature T, dT_f/dT, written mathematically in Eq. (5):

$$C_p^N = \left.\frac{dT_f}{dT}\right|_T = \frac{\left.(C_p - C_{p,g})\right|_T}{\left.(C_{p,l} - C_{p,g})\right|_{T_f}} \qquad (5)$$

C_p^N varies from zero in the glassy state at temperatures well below T_g, at which T_f does not depend on T (or $dT_f/dT = 0$), to one in equilibrium at temperatures well above T_g ($T_f = T$). The denominator of Eq. (5) $(C_{p,l} - C_{p,g})$, when the glass and liquid heat capacities are linearly dependent on temperature, is required to be determined at the fictive temperature. This T_f value can be evaluated using Eq. (6) [55]:

$$H(T_2) - H(T) = \int_{T}^{T_f} C_{p,g}(T')\,dT' + \int_{T_f}^{T_2} C_{p,l}(T')\,dT' \qquad (6)$$

The term $C_{p,g}(T)$ and $C_{p,l}(T)$ were replaced by $a + bT$ and $A + BT$, respectively. Then, Eq. (6) was integrated and rearranged into the form of a quadratic equation: $MT_f^2 + NT_f + Q = 0$. Therefore, T_f can be obtained from solving the quadratic equation with $M = 0.5(b - B)$, $N = a - A$, and $Q = AT_2 + 0.5BT_2^2 - aT - 0.5bT^2 - H(T_2) + H(T)$ where T_2 is the reference temperature, i.e. the temperature far above T_g at which the sugar is in equilibrium, and T is the temperature of interest. The difference in enthalpy at T_2 and T, $H(T_2) - H(T)$, was obtained by numerical integration of the experimental heat capacity data.

In order to obtain the TNM and Adam–Gibbs model parameters, the experimental normalized heat capacity data calculated using Eq. (5) were fit to the

model Equations (Eqs. (2) and (3), respectively). The calculated normalized heat capacity data were calculated using the response of fictive temperature to heating and cooling at a continuous rate $q = dT/dt$ based on the Boltzmann superposition. The response of T_f to q is given by Eq. (7) [2] when both non-exponentiality and non-linearity are taken into account:

$$T_f(T) = T_0 + \int_{T_0}^{T} dT' \left\{ 1 - \exp\left[\int_{T'}^{T} \left(\frac{dT''}{q\tau_0} \right)^{\beta} \right] \right\} \quad (7)$$

where T_0 is an initial temperature far above T_g at which the sample is at equilibrium. $T'$and T'' are dummy temperature variables. Eq. (7) was integrated numerically by treating cooling and heating as a sequence of temperature jumps ΔT followed by isothermal holds whose duration was determined by the cooling and heating rates q, $\Delta t = \Delta T/q$ [56]. The magnitude of ΔT used in all experiment was 1 K. Eq. (7) was then rewritten for n temperature jumps according to the Boltzmann superposition for unaged samples in the form:

$$T_{f,n} = T_0 + \sum_{j=1}^{n} \Delta T_j \left\{ 1 - \exp\left[-\left(\sum_{k=j}^{n} \frac{\Delta T_k}{q_k \tau_{0,k}} \right)^{\beta} \right] \right\} \quad (8)$$

Eqs. (2) and (3) were used as τ_0 in Eq. (8) for the TNM and Adam–Gibbs models, respectively.

In the case of the aged samples, the method of calculation of Hodge and Berens [56] was used. This was carried out by replacing the term $\Delta T_k/q_k$ in Eq. (8) with the aging time (t_a). The self-retarding kinetics of physical aging were accounted for by dividing the aging time into subintervals. To ensure linearity, the duration of the subinterval ΔT_k was small enough so that the decay of T_f was less than about 1 K. In this research, the duration of subintervals was 10 s for samples aged 60 min or below, 100 s for samples aged over 60–720 min, and 1000 s for samples aged over 720 min. T_f and τ_0 were calculated at the end of each subinterval. Since the value of q_k becomes zero during aging, the term $\Delta T_k/q_k$ cannot be calculated. To solve this problem, Eq. (8) was modified by holding the Boltzmann summation over j constant at the beginning of the aging time (n_A) while the summation over k is increased for each subinterval. Therefore, Eq. (8) for the aged samples becomes [11]:

$$T_{f,n} = T_0 + \sum_{j=1}^{n} \Delta T_j \left(1 - \exp\left(-\left(\sum_{k=n_A}^{n_A+n} \frac{\Delta t_k}{\Delta_{0,k}} \right)^{\beta} \right) \right) \quad (9)$$

The calculated C_p^N corresponding to Eq. (5) is given by:

$$C_p^N = \frac{dT_f}{dT} = \frac{T_{f,n} - T_{f,n-1}}{T_n - T_{n-1}} \quad (10)$$

The kinetic parameters of both models were obtained by a non-linear optimization technique via the Levenberg–Marquardt algorithm written in Fortran 90 [57]. The C_p^N for the experimental data (Eq. (5)) and calculated C_p^N (Eq. (10)) were minimized in order to obtain the best fit. The apparent activation energy, $\Delta h^*/R$ (in Eq. (2)) and Q (in Eq. (3)) were obtained from an independent experiment and used in the program as constants. The first guess value of both parameter x and β in the first loop of the optimization program was started at 0.5. The first guess value of the pre-exponential factor A was roughly estimated from Eq. (11). Eq. (11) was obtained by assuming τ_0 at T_g to be 100 s and $T_f \sim T$, and substituting these values into Eq. (2) [11]:

$$\ln A = -\frac{\Delta h^*}{RT_f'} + 4.6 \quad (11)$$

4. Results and discussions

4.1. The apparent activation energy (Δh^*)

The apparent activation energy, Δh^*, expresses the temperature dependence of the relaxation times near equilibrium. Δh^* can be estimated independently from either the heating or cooling rate (q_h, q_c) dependence of the limiting fictive temperature (T_f', the unaged fictive temperature) [16,20]:

$$\frac{-\Delta h^*}{R} = \frac{d \ln|q|}{d(1/T_f')} \quad (12)$$

where R is the ideal gas constant. The values of $\Delta h^*/R$ for each glass were determined from the thermal cycle described in the materials and methods section with equal cooling and heating rates, $q_h = |q_c| = |q|$. Four

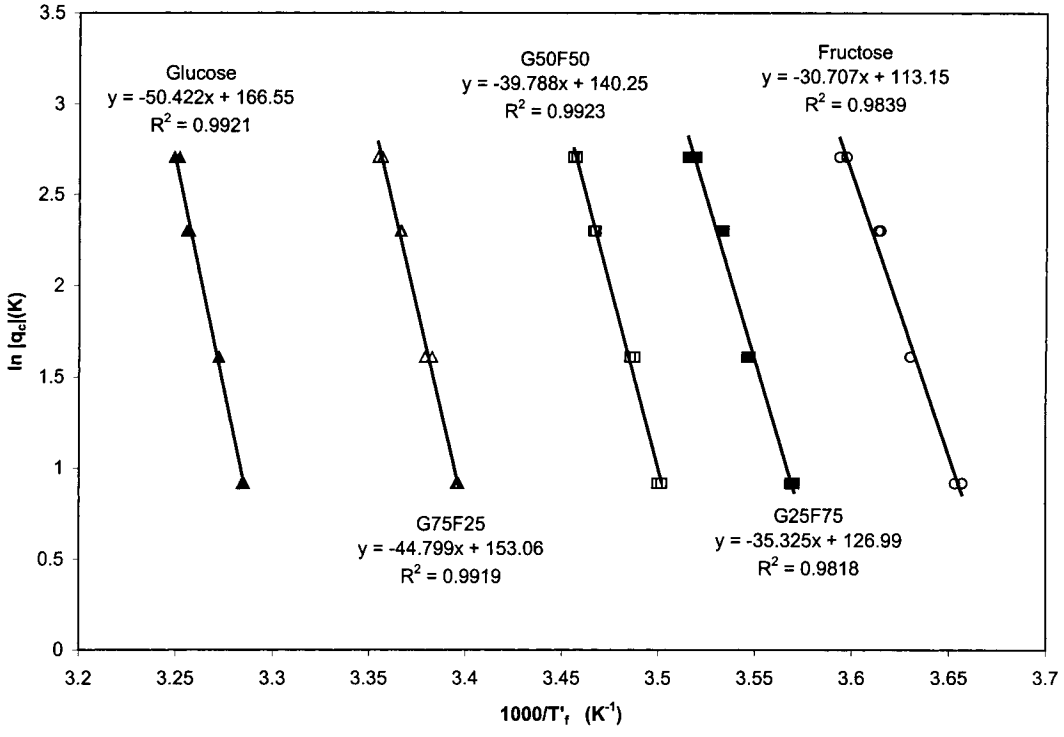

Fig. 2. Plot of logarithm of cooling rates ln $|q_c|$, versus reciprocal of the fictive temperatures T'_f for glucose, fructose and their mixtures. Points are experimental data, and solid lines are the best-fit lines. The slopes are the $\Delta h^*/R_{exp}$ values obtained according to Eq. (12).

heating rates were used, 2.5, 5, 10, and 15 K/min. Due to the limitation of the cooling system which uses helium as the cooling head purge gas and the low T_1 values needed (especially in the case of fructose), the maximum cooling rate possible was 15 K/min. The heating thermograms of the unaged sugars cooled and reheated at equal cooling and heating rates are given in Wungtanagorn [57]. The limiting fictive temperature (T'_f) was determined using the method of Richardson and Savill [58]. The least-squared values of $\Delta h^*/R$ for each sugar were determined by the slope of the plot of ln $|q_c|$ versus T'_f (Eq. (12)) and are shown in Fig. 2 and Table 1 ($\Delta h^*/R_{exp}$). The overall best-fit values of $\Delta h^*/R$ obtained by four-parameter optimization to the TNM model, are also reported in Table 1 ($\Delta h^*/R_{fit}$). It was found that the values obtained from the dependence of T'_f on the cooling rate were consistent with those obtained by four-parameter optimization to the

Table 1
Limiting fictive temperatures and apparent activation energies, $\Delta h^*/R$ of glucose, fructose and their mixtures[a]

Sugars	T'_f (K)	$\Delta h^*/R_{exp}$ (10^3 K)	$\Delta h^*/R_{fit}$ (10^3 K)	SS
Glucose	307.10 ± 0.116	50.422 ± 1.8646	48.995 ± 3.6779	0.022
G75F25	297.07 ± 0.042	44.799 ± 2.0739	42.509 ± 0.3646	0.018
G50F50	288.46 ± 0.058	39.788 ± 2.9281	39.610 ± 0.5744	0.006
G25F75	283.03 ± 0.045	35.325 ± 2.6163	35.234 ± 0.8021	0.004
Fructose	276.72 ± 0.071	30.707 ± 2.6651	29.790 ± 2.1627	0.006

[a] The subscript 'exp' indicates $\Delta h^*/R$ values were determined from the dependence of T'_f on cooling rate $|q_c|$ (Fig. 2). The fit subscript indicates $\Delta h^*/R$ values were obtained by four-parameter fitting (Eq. (2)) of the unaged thermograms to the TNM model, minimizing the sum of squares of the residuals (SS).

TNM model. However, the values from the optimization were slightly lower than those obtained via the $\ln |q_c|$ versus T'_f plot, which is in agreement with that reported by Hodge [11].

The value of $\Delta h^*/R$ decreased with increasing fructose content in the glass. It should be noted that the value of Δh^* is considered to be too large to be a simple transition state activation energy. The large values of Δh^* above T_g might be explained in terms of the cooperative translational molecular motions of many atoms so that the activation energy is shared by a large number of relaxing species [10].

Values of $\Delta h^*/R$ for other sugars have been reported in the literature, such as 78.5×10^3 K for maltose [14], 42.2×10^3 K for sorbitol, and 44.1×10^3 K for fructose [59] using equal heating and cooling rates in the range of 2.5–20 K/min. The values of $\Delta h^*/R$ increased to 86.12×10^3 and 84.44×10^3 K for sorbitol and fructose, respectively, when unequal cooling–heating rates were used, i.e. cooling at rates ranging from 1.25 to 20 K/min followed by heating at a fixed rate of 10 K/min [59]. The value of $\Delta h^*/R$ of fructose reported in the present study was somewhat lower than the value reported by Simatos et al. [59].

The difference in $\Delta h^*/R$ values reported here compared to the literature may be due to two factors, the decomposition and the relaxations above T_g in fructose. The former factor arises from the large difference in the melting temperatures of glucose and fructose. The onset melting temperatures of glucose and fructose were found at 431.44 K (158.24°C) and 386.78 K (113.58°C), respectively, which is about 45 K apart from each other. The large difference in melting temperatures of the sugars caused a portion of the fructose component in the mixtures to decompose before the glucose was completely melted. The decomposition of fructose may be responsible for the low value of Δh^*. The later factor arises from the complexity of the relaxation above T_g in molten fructose. Parameter Δh^* refers to the apparent activation energy in the equilibrium state above T_g. However, the fructose liquid obtained on fusion is initially not in the equilibrium state. Slow relaxation processes can occur in the liquid above T_g due to the coexist of at least six structurally distinct conformers of the fructose molecule; i.e. two anomer forms (α-fructopyranose and β-fructopyranose) of each of the $^1C_4$ and $^4C_4$, α-fructofuranose, and β-fructofuranose [60–62]. Each conformer has a different energy level. The composition of the conformers, the rate of tautomerization, and the equilibrium state of the liquid are a function of temperature with different time scales for equilibration [62].

Furthermore as pointed out by Hodge [11], a wide range of cooling rates is needed for accurate evaluation of T'_f for high values of Δh^*, because of the large uncertainties in T'_f, usually ± 0.5 K, for polymers. The limitation of the DSC cooling system and the low glass temperature of fructose confined the maximum cooling rate used in this research to 15 K/min.

4.2. TNM model parameters

The TNM model parameters ($\ln A$, x, and β; Eq. (2)) were determined using the Levenberg–Marquardt optimization procedure which minimizes the sum of squares of the residuals (SS) of the experimental and calculated normalized heat capacity data. The best-fit TNM parameters of the unaged sugars using the fixed $\Delta h^*/R_{exp}$ values obtained from the least squares values of $\ln |q_c|$ versus T'_f plot (Fig. 2; Table 1) are reported in Table 2. Fig. 3 shows the representative best-fit normalized heat capacity curves of the unaged thermograms of the sugars heated at 10 K/min using the TNM parameters in Table 2. The results show that the values of $\ln A$ and x increased with increasing fructose

Table 2
Best-fit TNM model parameters of unaged glucose, fructose, and their mixtures (Eq. (2)), minimizing the sum of squares of the residuals (SS)[a]

Sugars	ln A (s)	x	β	SS
Glucose	−159.43 ± 0.574	0.497 ± 0.0212	0.643 ± 0.0269	0.022
G75F50	−146.20 ± 0.021	0.516 ± 0.0086	0.570 ± 0.0054	0.018
G50F50	−133.55 ± 0.406	0.656 ± 0.0103	0.498 ± 0.0012	0.006
G25F75	−120.75 ± 0.049	0.717 ± 0.0257	0.472 ± 0.0085	0.004
Fructose	−106.96 ± 0.097	0.755 ± 0.0026	0.505 ± 0.0295	0.006

[a] The $\Delta h^*/R_{exp}$ values were used as a constant for each sugar reported in Table 1.

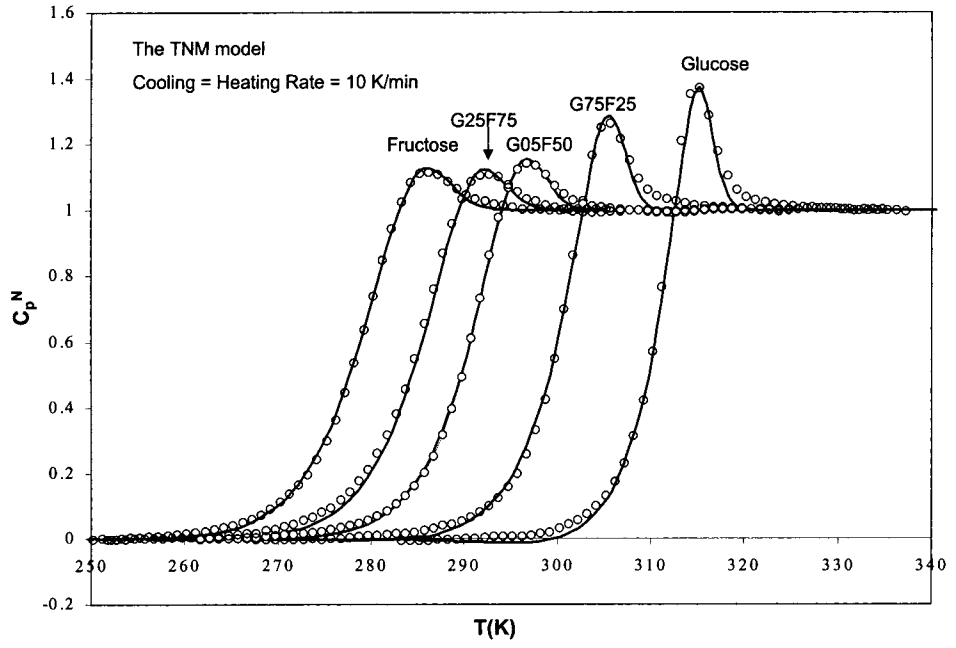

Fig. 3. Representative best-fit normalized heat capacity curves (solid lines) of unaged heating thermograms of glucose, fructose and their mixtures heated at 10 K/min using the TNM parameters in Table 2. Points are experimental data.

content. Whereas the values of β generally decreased as the fructose content increased. The overall fitting uncertainty in x and β for duplicates at a cooling-heating rate of 10 K/min was smaller than ± 0.03 which is consistent with results for polymer samples reported by others, about ± 0.05 for each parameter [10,20,63]. The pre-exponential factor A in the TNM model is the relaxation time in equilibrium at an infinitely high temperature. The magnitude of A is usually large in polymers and also in sugars as shown in Table 2. The value of A has no physical interpretation. However, the value of $\ln A$ is related to the values of Δh^*, for example, the change in $\ln A$ moves the dT_f/dt versus T curve along the T axis by an amount $\Delta T \approx (RT_g^2/\Delta h^*)\Delta \ln A$ [11].

The exponent β is a non-dimensional relaxation parameter, which is inversely proportional to the corresponding width of the relaxation-time distribution. Parameter β is equal to one for a single relaxation-time behavior or a single exponential decay. For relaxation of all materials, β is less than one. Smaller values of β correspond to an increase in the distribution of relaxation times. In glucose–fructose systems, the value of β was found to decrease from 0.643 in pure glucose to 0.498 in 50% fructose content. At higher ratios of fructose (over 50% fructose content), the value of β appeared to be unchanged within the range of the standard deviations. The average β values of the 50% fructose, the 75% fructose, and the pure fructose was 0.492 ± 0.021. The initial decrease in β, as the fructose content increased, reflects a broadening of the distribution of the enthalpy relaxation times. However, the width of the distribution of the relaxation times appeared to be unchanged when the fructose content was higher than 50%. A similar result was found for the AgI–$AgPO_3$ glass system in that AgI content decreased the width of the distribution of the relaxation times as the AgI content increased to 10% and additional AgI did not show a detectable effect on the distribution [64]. The value of β for smaller molecules is generally higher than that of polymers; for example the β for PVAc and PVC is about 0.27–0.41 and 0.11, respectively, whereas the β for small molecule such as LiCl is 0.68 [10,11]. The values of β for both glucose and fructose found in this research are similar to those reported for sucrose (0.4–0.8) [65], but in generally are higher than those reported for polymers [11]. In the case of polymers, the parameter β

was also interpreted as a measure of the degree of cooperativity defined in terms of the number of chain segments involved in a particular relaxation event [66]. Low values of β correspond to a high degree of cooperativity and a large number of chain segments resulting in a large activation energy for the relaxation event.

The non-linearity parameter x ($1 \geq x > 0$) defines the degree of non-linearity, i.e. the relative contributions of temperature and structure to the relaxation time. A value of x equal to one indicates that the relaxation time is due entirely to the absolute temperature of the system. On the other hand, a value of $1 - x$ defines the part of the relaxation time, which is dependent on the structural state of the system as characterized by the fictive temperature. Glucose has a value of x around 0.5 indicating that there is an equal temperature and structural state dependence. However, the temperature dependence became stronger (or the degree of non-linearity became weaker) as the amount of fructose increased as manifested by an increase in the value of x.

A strong correlation among the relaxation parameters A, Δh^*, x, and β obtained from the curve-fitting method and peak-shift method has been found for a variety of polymeric, organic, and inorganic glass even though these correlations are not clearly understood [10,30,66,67]. A high value of Δh^* is generally associated with low values of $\ln A$, β and x. A high value of x is generally associated with high values of β. This inverse correlation of Δh^* and $\ln A$ or x is in agreement with the results reported in this research, i.e. a high value of Δh^* for glucose was associated with low values of $\ln A$ and x as shown in Table 2. However, the β values in the glucose–fructose systems decreased as the x value increased, which is in contrast with the correlation of x and β for most polymers [10,66].

4.3. Adam–Gibbs model parameters

Like the constant value of $\Delta h^*/R$ in the TNM model, Q/R in the Adam–Gibbs model can be used in the fitting program as a constant. The analogous equation to Eq. (12) for the Adam–Gibbs equation can be expressed as [1,9]:

$$\frac{\mathrm{d}\ln|q_c|}{\mathrm{d}(1/T_f')} = -\frac{\Delta h^*}{R} = \frac{-Q}{R(1 - T_2/T_f')^2} \tag{13a}$$

or

$$\frac{Q}{R} = \frac{\Delta h^*}{R}\left(1 - \frac{T_2}{T_f'}\right)^2 \tag{13b}$$

The values of $\Delta h^*/R$ for each sugar were obtained from the slope of the plot of $\ln|q_c|$ versus T_f' ($\Delta h^*/R_{exp}$ reported in Table 1). The value of T_f' in Eq. (13b) for each sugar was set to the value of T_f' of the unaged thermogram at a heating rate of 10 K/min. The Adam–Gibbs model parameters ($\ln B$, T_2 and β, Eq. (3)) were determined using the Levenberg–Marquardt optimization procedure and are reported in Table 3. The representative best-fit normalized heat capacity curves of unaged sugars heated at 10 K/min using the Adam–Gibbs parameters are shown in Fig. 4. The Q/R_{fit} values were obtained by fitting the experimental normalized heat capacity data to the Adam–Gibbs model directly without using the known values of $\Delta h^*/R_{exp}$ from the cooling rate dependence of the limiting fictive temperature (Table 1). The Q/R_{cal} values were recalculated using Eq. (13b) with the fitted T_2 value. As can be seen from Table 3, the values of Q/R_{fit} and Q/R_{cal} are quite similar. It was found that Q/R increased with increasing fructose content. In contrast, the values of T_2 and β

Table 3
Best-fit Adam–Gibbs model parameters of unaged glucose, fructose, and their mixtures (Eqs. (3) and (13a)), minimizing the sum of squares of the residuals (SS)[a]

Sugars	$\ln B$ (s)	Q/R_{fit} (10^3 K)	Q/R_{cal} (10^3 K)	T_2 (K)	β	SS
Glucose	−75.469 ± 1.8611	11.876 ± 0.8766	12.000 ± 0.7027	157.327 ± 4.3656	0.650 ± 0.0284	0.021
G75F50	−72.712 ± 1.2461	12.111 ± 0.5635	11.771 ± 0.3747	144.806 ± 2.4174	0.576 ± 0.0052	0.017
G50F50	−85.445 ± 0.9247	16.740 ± 0.1448	16.873 ± 0.4992	100.620 ± 2.7787	0.501 ± 0.0007	0.006
G25F75	−85.0034 ± 2.9528	17.918 ± 0.5951	17.999 ± 1.2131	81.0567 ± 6.8104	0.475 ± 0.0077	0.003
Fructose	−79.1533 ± 0.3204	17.707 ± 1.2872	17.246 ± 0.172‘5	69.342 ± 1.0368	0.508 ± 0.0295	0.041

[a] Q/R_{fit} was obtained from four-parameter fitting (Eq. (3)) and Q/R_{cal} was obtained by recalculating using Eq. (13b) with $\Delta h^*/R_{exp}$ values reported in Table 1.

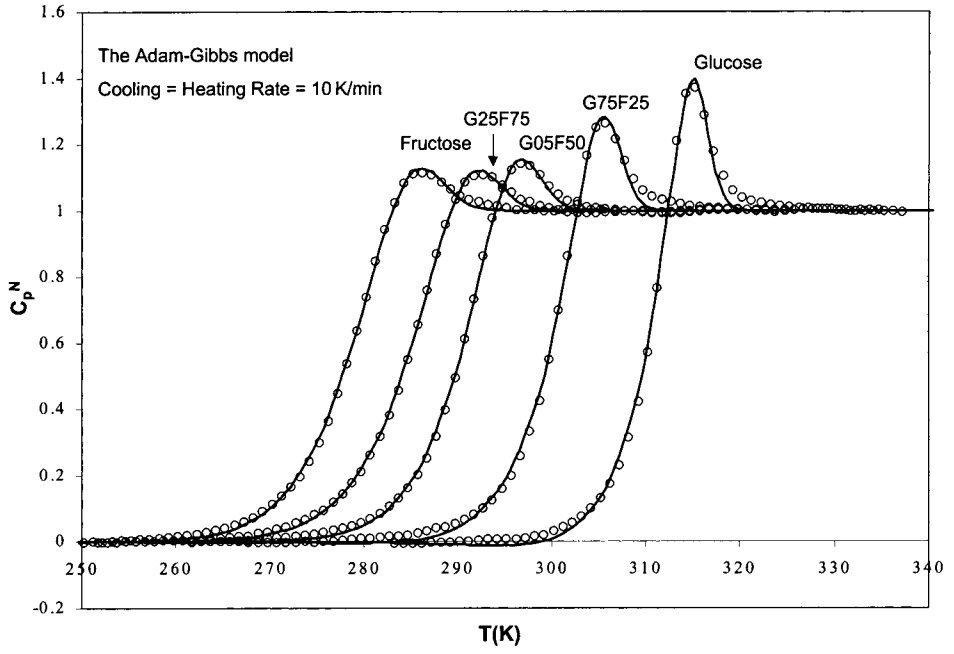

Fig. 4. Representative best-fit normalized heat capacity curves (solid lines) of unaged heating thermograms of glucose, fructose and their mixtures heated at 10 K/min using the Adam–Gibbs parameters in Table 3. Points are experimental data.

decreased as the fructose content increased. No trend between ln B and the fructose content was observed. The values of β from the Adam–Gibbs model were found to be consistent with those found for the TNM model within the range of the standard deviation.

The values of T_2 obtained from the Adam–Gibbs model using the enthalpy relaxation data have been found to be very similar to the Kauzmann temperature T_K for some materials, such as As_2Se_2 and B_2O_3 [10]. The values of T_2, therefore, may be used to estimate the value of T_K for the sugars (even though there are some polymers such as polystyrene for which T_2 is somewhat different than T_K). The approximate relation between the TNM and Adam–Gibbs parameters was derived from the temperature derivatives of τ in the equilibrium ($T_f = T$) state and the glassy ($T_f = T_f'$) state as reviewed in detail by Hodge [11]. The approximated values of parameter x can be found by the relation of x and T_2 expressed as [9]:

$$x \approx 1 - \left(\frac{T_2}{T_f'}\right) \tag{14}$$

The x values calculated using Eq. (14) for the Adam–Gibbs model are shown in Table 4 and can be compared to the x values for the TNM model (Table 2). It was found that the x values for the sugars obtained from the TNM model were in agreement with those obtained from the Adam–Gibbs model via Eq. (14) within the same standard deviation. According to Eq. (14), the values of parameter x indicates the proximity of T_f' to T_2 [10]. In an unaged sample, T_f' approximately equals T_g and T_2 approximately equals T_K. The relation between x and T_K/T_g, therefore, suggests that non-linearity is determined by how close

Table 4
The values of the parameter x for the Adam–Gibbs model calculated using the Eq. (14)[a]

Sugars	x, Adam–Gibbs model	$T_{g,\ inflection}$ (K)	$T_g - T_2$ (K)
Glucose	0.488 ± 0.0142	312.01 ± 1.093	154.68
G75F25	0.513 ± 0.0081	301.66 ± 0.120	156.86
G50F50	0.651 ± 0.0096	292.76 ± 0.481	192.14
G25F75	0.714 ± 0.0241	286.93 ± 0.467	205.87
Fructose	0.749 ± 0.0038	280.06 ± 0.191	210.72

[a] T_g inflection and $T_g - T_2$ values of glucose, fructose and their mixtures. Inflection glass transition temperatures were obtained from the TA Analysis Solution software [51].

the kinetic T_g is to the thermodynamic T_K [68]. As T_g approaches T_2 and the number of thermally accessible configurations is reduced, the relaxation time becomes increasingly dependent on structure and x decreases, i.e. more non-linear [23]. As shown in Table 4, $T_g - T_2$ decreased from pure fructose to pure glucose and was associated with a decrease in the values of x, supporting the statement by Hodge [23].

4.4. Evaluation of parameter x using the peak-shift method

In addition to the curve-fitting method, the non-linearity parameter x can be determined via the dependence of the peak temperature T_p on four experimental variables (heating rate q_h, cooling rate q_c, aging temperature T_a, and the enthalpy loss δ_H). This is referred to as the peak-shift method. If three of the variables are keep constant, the effect of only one variable on the peak T_p can be found. The dependence of the peak T_p on each of these experimental variables are quantified as peak shifts, which are normalized to give dimensionless quantities [24,26–29,69]. For example, in this research, the effect of the heating rate on the temperature shift was evaluated and is defined in Eq. (15):

$$\hat{s}(Q_h) = \theta\left(\frac{\partial T_p}{\partial \ln q_h}\right)_{q_c,T_a,\delta_H} = \theta(m_{q_h}) \tag{15}$$

where θ is a material parameter characterizing the temperature dependence of the relaxation times at equilibrium [69] and m_{q_h} is the slope of the plot of T_p and $\ln q_h$.

The effects of each variable on the temperature shift actually are interrelated and depend critically on the non-linearity parameter x as expressed for the dependence of T_p on the heating rate in Eq. (16) (in which the cooling rate, the aging temperature and aging time were keep constant) [26,28,29]:

$$\hat{s}(Q_h) - 1 = F(x) \tag{16}$$

Theoretically, the dependence of $F(x)$ on x has been shown to be essentially independent of the distribution of relaxation times and the function $F(x)$ approaches a simple hyperbola (Eq. (17)):

$$\lim F(x) \to f(x) = (x^{-1} - 1) \tag{17}$$

The values of θ and activation energy, $\Delta h^*/R$, are related and can be obtained using the dependence of the limit fictive temperature, T_f', on the cooling rate, q_c (Eq. (18)) [38]. According to Eq. (18), the value of θ for each sugar can be determined from the slope of the best-fit line:

$$\frac{d \ln |q_c|}{dT_f'} = \theta = \frac{\Delta h^* c}{R T_f'^2} \tag{18}$$

The plot of $\ln |q_c|$ versus T_f' is shown in Fig. 5. Similarly to $\Delta h^*/R$, the value of θ decreased from glucose (0.538) to fructose (0.404) (Table 5). The degree of temperature dependence and the enthalpy relaxation rates are controlled mainly by the parameter $(1-x)\theta$. Materials with higher values of parameter $(1-x)\theta$ exhibited a low relaxation rate, such as vinylic polymers PVC, and vice versa for the lower values of $(1-x)\theta$ as in As_2S_3 or inorganic glasses [70,71]. If we consider the parameter $(1-x)\theta$ of the sugars in Table 5 (using the TNM x values from Table 2), the enthalpy relaxation rate of glucose is expected to be higher than that of fructose.

The dependence of the peak temperature, T_p, on the heating rate, q_h, was evaluated by using five heating rates of 2.5, 5, 10, 15 and 20 K/min with a fixed cooling rate of 10 K/min. The heating thermograms of each aged sugar at an aging temperature about 10 K below its T_g for 720 min and rescanned at the five heating rates are giving in Wungtanagorn [57]. The aging temperatures are shown in Table 6. The plot of T_p versus $\ln q_h$ is shown in Fig. 6. A linear dependence of the peak temperature and the heating rate was found. The slopes m_{q_h} of the plot for each sugar are shown in Table 6, along with the values of the shift,

Table 5
Parameter θ obtained from the plot in Fig. 5 with regression coefficient R^2, parameter $(1-x)\theta$ of glucose, fructose and their mixtures[a]

Sugars	θ	$(1-x)\theta$
Glucose	0.538 ± 0.0204	0.271
G75F25	0.510 ± 0.0241	0.247
G50F50	0.481 ± 0.0354	0.166
G25F75	0.444 ± 0.0148	0.126
Fructose	0.404 ± 0.0349	0.099

[a] The non-linearity parameter x values are obtained from fitting to the TNM model (Table 2).

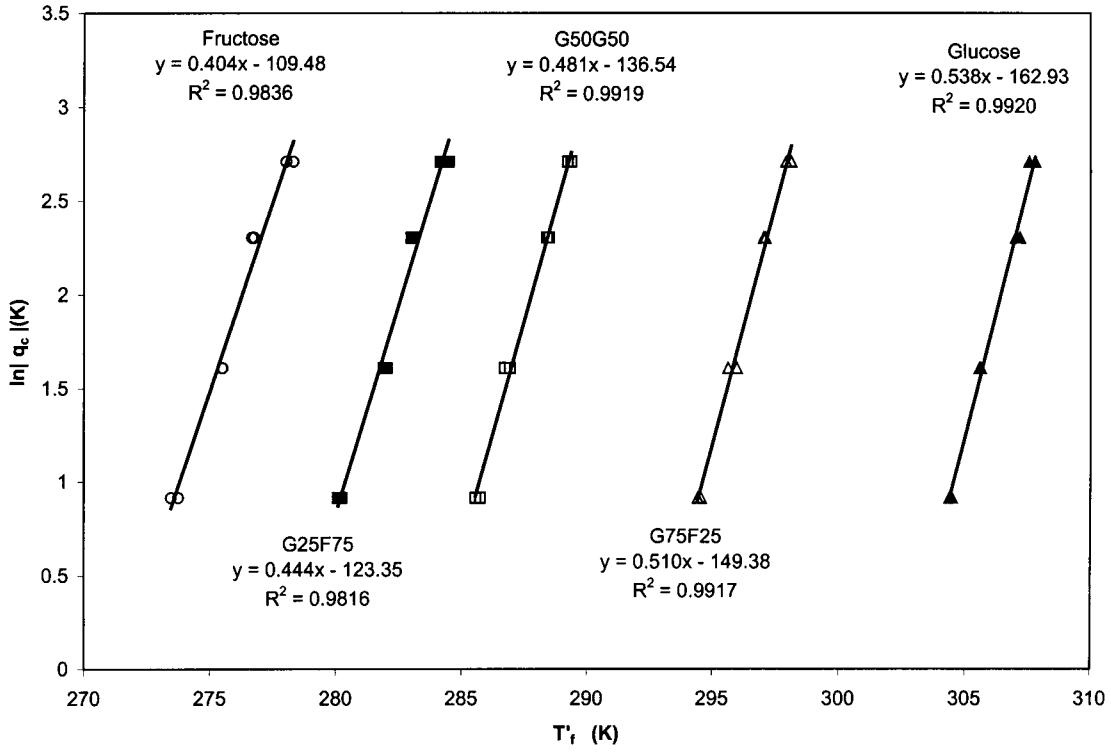

Fig. 5. Plot of ln $|q_c|$ vs. T_f' of glucose, fructose and their mixtures. The least squared values of θ for each sugar were determined by the slope of the plot of ln $|q_c|$ vs. T_f' (Eq. (18)).

$\hat{s}(Q_h)$ obtained from the multiplication of the m_{q_h} and θ (Table 5) according to Eq. (15).

The values of the parameter x for each sugars were obtained via the $f(x)$ function in Eqs. (16) and (17). Since the peak temperature T_p depends on the cooling (q_c) and heating rate (q_h) a correction for thermal lag is required before applying the peak-shift method [72]. Theoretically, the unaged endotherm of the same cooling-heating rate ratio should have the same peak width. The correction can be done by adjusting the peak position with a scaling factor, $F_{q_c} = W_{10}/W_{q_c}$, where W_{10} is the peak width of the reference heating rate, for example at 10 K/min, and W_{q_c} is the peak width at other cooling rates. However, in this experiment, the peaks of the unaged sugar thermograms were very small. The peak became smaller with the addition of fructose and at lower cooling-heating rates. Therefore, the values of the T_p peaks used for the plot in Fig. 6 were obtained from the thermograms without taking the thermal lag effect into account. However, as

Table 6
Aging temperatures T_a, slope m_{q_h} of the linear regression of the peak temperatures versus the logarithm of the heating rate, the values of $\hat{s}(Q_h)$ shift, and parameter x calculated from $\hat{s}(Q_h)$ for glucose, fructose and their mixtures

Sugars	T_a (K)	m_{q_h}	$\hat{s}(Q_h)$	x, $\hat{s}(Q_h)$
Glucose	301.2	3.348 ± 0.1014	1.784 ± 0.0134	0.553 ± 0.0041
G75F25	289.7	3.160 ± 0.1690	1.613 ± 0.0090	0.629 ± 0.0036
G50F50	282.7	3.180 ± 0.1282	1.531 ± 0.1747	0.653 ± 0.0740
G25F75	277.7	3.154 ± 0.1247	1.398 ± 0.1008	0.734 ± 0.0541
Fructose	271.2	2.999 ± 0.0303	1.210 ± 0.1171	0.824 ± 0.0791

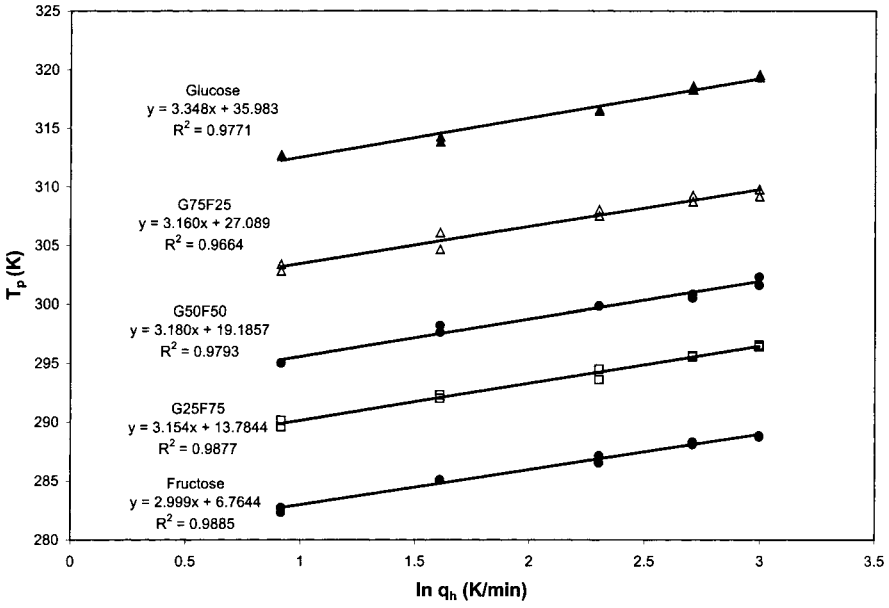

Fig. 6. Heating rate dependence of the peak temperature of the sugar glasses. Heating rates of 2.5, 5.0, 10, 15, and 20 K/min were used. Aging temperatures for glucose, G75F25, G50F50, G25F75, and fructose were 301.2, 289.7, 282.7, 277.7, 271.2 K, respectively. Aging time and cooling rate were fixed at 720 min 10 K/min, respectively. The slopes are the m_{q_h} values obtained according to Eq. (15).

shown by Hutchinson et al. [72], the dependence of T_p on the cooling rate is far from linear relation if a wide range of cooling or heating rates was chosen. In order to minimize the thermal lag effect, the maximum cooling and heating rates were limited to 20 K/min. The regression coefficients (R^2) of the linear squares fit shown in Fig. 6 were very close to one.

The values of parameter x obtained from the peak-shift method (Table 6) followed the same trend as those obtained by the curve-fitting method (for the TNM (Table 2) and Adams–Gibbs models (Table 4)), i.e. parameter x increased as fructose content increased. However, the values found by the peak-shift method were higher than those found by the curve-fitting method. The higher value of x may be due to the lack of the thermal-lag correction and/or from using the function $f(x)$ instead of $F(x)$. The function $F(x)$ was actually derived from the spectrums of relaxation times such as single box or double box spectrums. The function $f(x)$ is believed to be very close to the upper limit of $F(x)$. The value of x estimated from Eq. (17) was found to be higher than its actual value by approximately 0.05–0.1 and the range of uncertainty was determined by the degree of aging before reheating [29]. If the uncertainty of 0.05–0.1 is taken into account, the values of x from both methods yield similar results. The peak-shift method, therefore, allows the parameter x to be determined directly and simply from the theoretically calculated variation of the $f(x)$ curve (Eq. (17)) without any assumptions about the form of the relaxation time distribution.

The function $F(x)$ is essentially independent of the distribution function and of other material parameters, such as θ and ΔC_p. The value of $F(x)$, however, is sensitive to the parameter x, particularly within the range $0.2 < x < 0.6$. The parameter x values for glucose obtained from both curve-fitting and peak-shift methods fall within this range, but that for fructose slightly exceeds this range. The peak-shift method, therefore, may yield more accurate results for glucose or glucose–fructose mixtures than pure fructose.

4.5. Fragility index (m)

The "strong/fragile liquid" classification for liquids was proposed by Angell [15,39–45]. Angell and cowokers used this concept to classify supercooled

materials into "strong" and "fragile" liquids according to the change in their dynamic properties, such as viscosity, in the temperature range above T_g. In other words, this strong/fragile liquid classification is an indicator of the sensitivity of the liquid structure to temperature changes. The concept of fragility was simplified for systems near the glass transition temperature by introducing a parameter called "the fragility m" index [44,45,48,73]. The fragility index is defined as the slope at the T_g of the T_g-scaled (T_g/T) Arrhenius plot of any relaxation time parameter, such as the log of the viscosity (which is proportional to the relaxation times) versus T_g/T. Therefore, the classification is based on the different responses of amorphous materials with different molecular structures to changes in temperature. Strong liquids, such as SiO_2 and GeO_2, exhibit Arrhenius temperature-dependent behavior (a nearly linear dependence of the log of its relaxation times or viscosity on the inverse of temperature, i.e. the slope does not change much when temperature increases above T_g). Strong liquids typically show a very small jump in C_p and a low activation energy at T_g. Fragile liquids, such as *o*-terphenyl, on the other hand, exhibit non-Arrhenius temperature dependent behavior and a rapid decrease in viscosity with increasing temperature. Fragile liquids typically show a very large jump in C_p and a very high apparent activation energy at T_g [15,39,41]. Based on the definition of the fragility index m is defined in terms of the activation energy Δh^* [74]:

$$m = -\frac{\Delta h^*}{2.303RT_g} \tag{19}$$

Simatos et al. [75] recommended T_g inflection (Table 4) as the T_g value used in Eq. (19).

The fragility index values calculated from the activation energy via Eq. (19) are given in Table 7. The fragility index decreased systematically from 70.2 in glucose to 47.6 in fructose indicating that glucose was more fragile than fructose, moreover, an addition of fructose decreased the fragility of the mixtures.

The strong-fragile concept actually describes the temperature dependence of the viscosity or average relaxation times in the equilibrium liquid [25]. The interpretation of the glassy relaxation behavior using the strong-fragile classification was attempted via the correlation of fragility with both characteristics of relaxation, non-linearity and non-exponentaility. Parameter x, usually characterized as the degree of non-linearity, was found to exhibit an inverse correlation with fragility in some glass-forming polymers [25,48]. The inverse correlation of m and x is consistent with the values of x in Tables 2, 4 and 6 and m (calculated from Eq. (19)) in Table 7. The higher value of x in fructose is associated with a lower value of m, compared to those same values in glucose. The addition of fructose produced a stronger liquid, which exhibited more Arrhenius temperature-dependent behavior than pure glucose. The mixtures tended to deviate from Arrhenius behavior and became more fragile as the glucose content increased.

The correlation of the parameters m and x is described using Eq. (20) [48]:

$$m = \frac{m_{\min}}{\vartheta(x-1)+1} \tag{20}$$

where $m_{\min}$ equals 16 and $\vartheta = T_f'/T_g \geq 1$. Eq. (20) reduces to $m = m_{\min}/x$ for $T_f = T_g$. Experimentally, Eq. (20) has been shown to hold for values of ϑ which range between 1.0 and 1.2 ($1.0 \leq \vartheta \leq 1.2$). The estimate of $m_{\max}$ is about 200 based on the statistics of Voronoi polyhedra [47]. If a scale of 16 ($m_{\min}$) to 200 ($m_{\max}$) is used, both glucose and fructose are considered to be on the strong side of the scale.

The values of $\vartheta = T_f'/T_g$ for the sugars are reported in Table 7, where T_g is the onset glass transition temperature. Eq. (20) was used to calculate the fragility index values using $\vartheta = T_f'/T_g$ and the non-linearity parameter x obtained from the TNM (Table 2) and Adam–Gibbs (Table 4) models and the peak-shift method (Table 6). Although the values of ϑ calculated from T_f'/T_g were in the range of 1.0–1.2, the values of the fragility index calculated from Eq. (20) (Table 7, m_{TNM}, $m_{Adam–Gibbs}$, $m_{\hat{s}}(Q_h)$) were only about half of the m obtained using the activation energy (Table 7, Eq. (19)). When the values of ϑ_{TNM}, $\vartheta_{Adam–Gibbs}$, and $\vartheta_{\hat{s}q_h}$ are calculated via Eq. (20) using their respective non-linearity parameter x values and m values obtained from the activation energy ($\Delta h^*/R$) calculation (Table 7, Eq. (19)), the values of ϑ_{TNM}, $\vartheta_{Adam–Gibbs}$, and $\vartheta_{\hat{s}q_h}$ exceeded the effective range of ϑ found for Eq. (20). The plot of the fragility index m determined from the activation energy (Table 7, Eq. (19)) versus the non-linearity parameter x for all samples obtained from the TNM and Adam–Gibbs models and from the peak-shift

Table 7
Fragility index (m) calculated from Eq. (19), onset glass transition temperature $T_{g\ onset}$, the ratio of T_f' and $T_{g\ onset}$ (ϑ), and fragility index m using Eq. (20) with the values of parameter x obtained from the TNM and Adam–Gibbs models, and the peak-shift method[a]

Sugars	Fragility index, m	$T_{g\ onset}$ (K)	$\vartheta = T_f'/T_g$	m_{TNM}	$m_{Adam–Gibbs}$	$m_{\hat{s}}$	ϑ_{TNM}	$\vartheta_{Adam–Gibbs}$	$\vartheta_{\hat{s}}$
Glucose	70.171 ± 0.2460	307.92 ± 1.384	0.997 ± 0.0045	32.14 ± 1.431	32.75 ± 1.086	28.85 ±0.213	1.54±0.065	1.51 ± 0.041	1.73 ± 0.016
G75F25	64.486 ± 0.0257	296.79 ± 0.092	1.001 ± 0.0003	31.05 ± 0.528	31.25 ± 0.506	25.47 ±0.144	1.55±0.035	1.54 ± 0.026	2.02 ± 0.019
G50F50	59.012 ± 0.0969	287.15 ± 0.544	1.004 ± 0.0019	24.47 ± 0.413	24.64 ± 0.392	24.72 ±2.822	2.12±0.062	2.09 ± 0.056	2.15 ± 0.459
G25F75	53.458 ± 0.0870	280.51 ± 0.863	1.009 ± 0.0031	22.40 ± 0.841	22.52 ± 0.797	21.94 ± 1.639	2.49±0.225	2.46 ± 0.205	2.69 ± 0.546
Fructose	47.610 ± 0.0325	274.08 ± 0.615	1.010 ± 0.0023	21.26 ± 0.090	21.42 ± 0.125	19.56 ± 1.899	2.71±0.028	2.65 ± 0.039	4.19 ± 1.877

[a] The values of ϑ_{TNM}, $\vartheta_{Adam–Gibbs}$, and $\hat{s}(Q_h)$ were recalculated using Eq. (20) with the values of m (calculated from Eq. (19), column one above) and parameter x obtained from the TNM model, Adam–Gibbs model, and the peak-shift method.

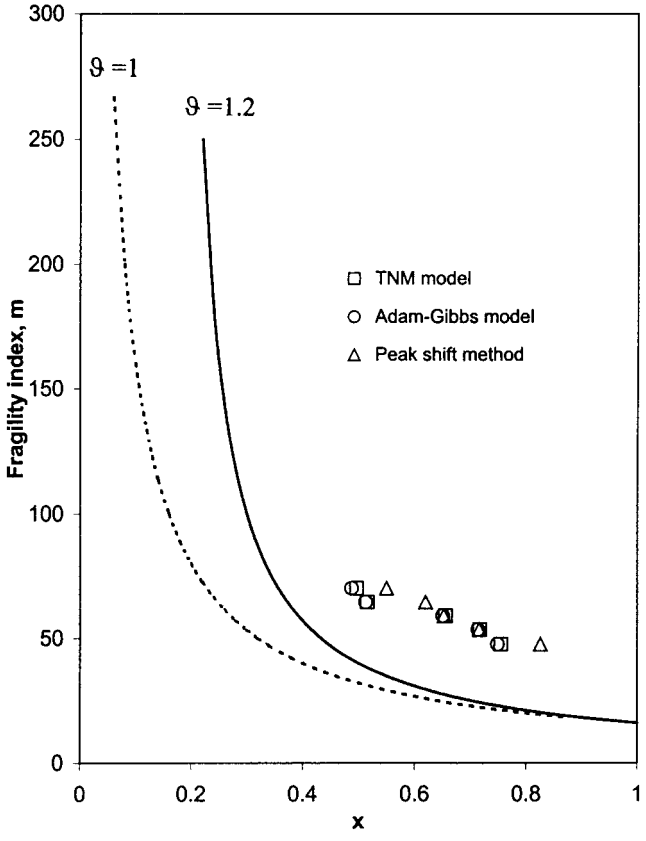

Fig. 7. Fragility index m determined from the activation energy ($\Delta h^*/R$, Eq. (19)) vs. non-linearity parameter x of all samples obtained from the TNM and Adam–Gibbs models and from the peak-shift method. The dash line and the solid line were calculated according to Eq. (20) with the values of $\vartheta = 1$ and $\vartheta = 1.2$, respectively.

method is shown in Fig. 7. The dash line and the solid line were calculated according to Eq. (20) with the values of $\vartheta = 1$ and 1.2, respectively. The fragility indexes are not in the range that Eq. (20) can predict accurately (between dash and solid lines). Eq. (20), therefore, might not be appropriate for describing the relation of the non-linearity parameter x and the fragility index in the glucose–fructose system. The values of m and x for some polymers do not follow Eq. (20), such as poly(stylene) — PS, poly-(vinylacetate) — PVAc, and $75Pb(PO_3)_2$–$25Fe_2O_3$ [48]. However, the expected trend between x and m for the sugar systems studied was still observed, i.e. the value of m decreased as the parameter x increased.

The general correlation between the non-exponentiality parameter β and fragility index m is also expected and shown by some materials [25,47,48,76]. Using the data for m and the width of the relaxation time distribution of 70 glass forming materials, Bohmer [48] showed that a fragile liquid (high value of m) is expected to have a broader distribution of relaxation times (low value of β) compared to a strong liquid. The glucose–fructose system, however, does not show the inverse correlation of m (Table 7, Eq. (19)) and β (TNM in Table 2 and Adam–Gibbs in Table 3). It should be pointed out here that the change in β with increasing fructose content is considered to be small, particularly when the fructose content is over 50% (compared to a wider range in β among 70 glass forming materials) and the m value of glucose is considered to be close to that of fructose (on a scale of 16–200). Therefore, the glucose–fructose system does not show the clear correlation of m and β as found in polymers.

Although the relaxation data can be used for evaluating the fragility, different types of relaxation data may not yield the same fragility index. If the Vogel–Tammann–Fulcher (VTF) parameters (T_0 and B) are known, it is possible to calculate the fragility index from Eq. (21) [42,44,45]:

$$m = 16 + \frac{590T_o}{B} \qquad \text{(relaxation time)} \tag{21a}$$

$$m = 17 + \frac{666T_o}{B} \qquad \text{(viscosity)} \tag{21b}$$

Eq. (21a) and (21b) are used for the quantities under analysis on the relaxation time data and viscosity data, respectively. The term B/T_o is called the strength parameter D which is related to m, i.e. a strong liquid has a large D and a fragile liquid has a small D [44,45,48,75].

Using the viscosity data from the paper of Ollett and Parker [77], Angell et al. [44,45] noted that fructose was stronger than glucose; with values of m being 105 ($B = 1926$ and $T_o = 256$) and 80 ($B = 2391$ and $T_o = 227$) for glucose and fructose, respectively. These values are somewhat larger than those obtained in this research, but both results show the same trend; i.e. the fragility index m of glucose is higher than that of fructose.

Perez and Cavaille [78] proposed another parameter m^* which is similar to m proposed by Angell [15]; m^* is calculated from the difference between the apparent activation energies at above and below T_g:

$$m* = \frac{\Delta h^{*T>T_g} - \Delta h^{*T<T_g}}{RT_g} \tag{22}$$

The values of $\Delta h^{*T>T_g}$ and $\Delta h^{*T<T_g}$ are obtained from the VFT parameters B and T_o:

$$\Delta h^{*T<T_g} = \frac{BRT_g}{(T_g - T_o)} \tag{23a}$$

$$\Delta h^{*T<T_g} = \frac{BRT_g^2}{(T_g - T_o)^2} \tag{23b}$$

By using the VTF parameters from the paper of Ollett and Paker [77] ($B = 1926$ K, $T_o = 256$ K, $T_g = 304$ K for glucose and $B = 2391$ K, $T_o = 227$ K, $T_g = 283$ K for fructose), m^* was calculated as 214 for glucose and 173 for fructose. The values of m^* are very large compared to the values of m but still give the same prediction that fructose is somewhat stronger than glucose.

The discrepancy in the m values between the literature and this study may arise from the difference in the type of relaxation data used, i.e. viscosity, dielectric and enthalpy relaxation data, and the means of calculation. Another example is found for sorbitol. The value of m for sorbitol calculated by Simatos et al. [59] via the parameter B and T_o of the Vogel–Tammann–Fulcher equation using the viscosity data of Angell and Smith [79] was about 94 which is similar to the value calculated from the dielectric relaxation data, 93 [74] but different from the value determined by mechanical spectroscopy which was 49 [59]. With the same methods used in the present paper, Simatos et al. [59] determined the fragility parameter from the activation energy Δh^* (obtained from the plot of $\ln q_c$ versus $1/T_f'$) and found that the value of the fragility parameter (m) was about 66–81 in sorbitol and about 66–71 in fructose. The higher value of fragility in fructose was associated with the higher value of Δh^* compared to the Δh^* obtained in this research. The difference in the value of Δh^* has been discussed earlier in Section 4.1.

Besides using relaxation data (activation energy and non-linearity parameter x) to determine the fragility of a material, other parameters such as ΔC_p or $C_{p,l}/C_{p,g}$ and melting point to glass transition ratios (T_m/T_g) can also be used as indicators to classify the strong and fragile liquids. Strong liquids tend to have a small jump in heat capacity or a low value of $C_{p,l}/C_{p,g} < 1.1$ at T_g, a value of T_m/T_g (in K) of 1.5 or greater, and vice versa for fragile liquids [9,10,43–45,59]. In this research, the melting points of glucose and fructose were found at 431.144 ± 0.11 and 386.78 ± 0.32 K, respectively. Using the inflection glass transition temperatures in Table 4, the ratio of T_m/T_g for glucose and fructose were found to be virtually the same (Table 8). Both sugars also had the same ΔC_p at T_g midpoint (Table 8) and there was no trend observed in the values of ΔC_p (Table 8) or $C_{p,l}/C_{p,g}$ (Table 8). The values of T_m/T_g for both sugars are less than 1.5 and the values of ΔC_p are higher than for typical polymers, e.g. 0.28 J/g K for polystyrene [80]. Although the distinction between the sugars was not obvious from $C_{p,l}/C_{p,g}$ or T_m/T_g, both sugars could be considered as fragile liquids compared to other typical polymers. This is the opposite conclusion reached when m was

Table 8
Melting point T_m, the ratio of the melting point to the inflection glass transition temperature T_m/T_g of glucose and fructose and the change in heat capacity ΔC_p, ratio of liquid to glass heat capacity $C_{p,l}/C_{p,g}$, and the ratio of the T_2 to limiting fictive temperature T_2/T_f' of glucose and fructose and their mixtures

Sugars	$T_{m\ onset}$ (K)	T_m/T_g	ΔC_p (J/g K)	$C_{p,l}/C_{p,g}$	T_2/T_f'
Glucose	431.44 ± 0.106	1.383	0.77 ± 0.022	1.65 ± 0.172	0.512
G75F25	–	–	0.75 ± 0.020	1.59 ± 0.058	0.488
G50F50	–	–	0.78 ± 0.018	1.65 ± 0.088	0.349
G25F75	–	–	0.77 ± 0.015	1.62 ± 0.058	0.286
Fructose	386.78 ± 0.318	1.381	0.77 ± 0.014	1.61 ± 0.070	0.251

calculated using the relaxation data (Eqs (19) and (20)).

The paradox in interpreting the fragility of a material when using the relaxation parameters versus the heat capacity and T_m/T_g data has been previously reported. For instance, ΔC_p at the glass transition is larger for sorbitol than for fructose, 1 J/g K for sorbitol and 0.7 J/g K for fructose [59], based on those values it could be predicted that sorbitol would be more fragile than fructose; but both sugars have a similar fragility index as calculated from the apparent activation energy. A similar situation was found for cured epoxy resin. Hutchinson et al. [34] found that partially cured resin and fully cured resin had the same parameter x values obtained by the peak-shift method (implying no change in fragility) but there was an increase in the value of ΔC_p as the degree of curing decreases (implying an increase in fragility). There is still has no fully satisfying explanation for this paradox.

The ratio of T_2/T_f' (or T_K/T_g) from the Adam–Gibbs model is also a measure of fragility [68]; i.e. more fragile liquids would produce more non-Arrhenius glasses with higher T_2/T_f'. The values of T_2/T_f' (Table 8) along with the values of the parameter x (Table 4) predicted that glucose was more fragile (higher T_2/T_f') and more non-linearity (lower values of x) than fructose.

4.6. Cooling–heating rate and aging effects

The TNM and Adam–Gibbs model parameters of unaged sugars using the same thermal history as the data in Tables 2 and 3 but at equal heating and cooling rates of 15 K/min, instead of 10 K/min were also obtained (data available in Wungtanagorn [57]). In addition, the TNM and Adam–Gibbs model parameters of aged G50F50 at two aging temperatures, 282.7 and 272.7 K, were also obtained (data available in Wungtanagorn [57]).

It was clearly found that the cooling-heating rate and aging time affected the model parameters of both the TNM and Adam–Gibbs models. The increase in cooling–heating rate yielded an increase in T_f', Q/R, ln B, and the non-linearity parameter x for both models, but a decrease in T_2 and β. The value of ln B generally increased with fructose content, which was more clearly observed at a cooling-heating rate of 15 K/min compared to that at 10 K/min. The value of ln A, however, was not influenced by the cooling–heating rate. Theoretically, the value of ln A is associated with the value of Δh^* via Eq. (11). Since the $\Delta h^*/R_{exp}$ values were used as a constant in fitting, the ln A values only changed slightly. O'Reilly and Hodge [81] also found that both x and β decrease with increasing heating rate in polystyrene. At low heating rates (1.25–5 K/min where thermal gradients in the sample and thermal resistances are believed to be negligible), x and β both changed significantly with thermal history which contradicts the original assumption of the models that both x and β are material constants. They suggested that the TNM and KAHR models were deficient for polymers and the models might be defective at the higher cooling-heating rates as well.

Aging also influenced the model parameters. In glucose–fructose systems, the values of parameter x, β and Q/R were generally found to decrease as aging time increased, while the values of ln A, ln B, and T_2 increased with aging time. By comparing two aging temperatures for the G50F50 sample, it was found that the higher aging temperature resulted in higher values for x and β. The increase in the x value as a

function of aging time and temperature was also found in polymers such as poly(methyl methacrylate) aged at 375 and 387.5 K [55] and aged at 311, 362 and 380 K [16], and in inorganic glass such as $Li_2O{\cdot}2SiO_2$ [82]. However, there is a controversy in the change in the β value due to thermal history. For example, the β value of poly(methylmethacrylate) increased with aging time and temperature in the research by Cowie and Ferguson [55], but remain unchanged in the research by Tribone et al. [60]. No change in the β value with aging time and temperature was also found in $Li_2O{\cdot}2SiO_2$ [82] which confirms that the thermorheological simplicity assumption of the model was not violated. The variance of the fitting of the raw data appeared to increase with aging time and temperature in this research (by comparing the sum of squares (SS) values as the aging time or aging temperature increased). Tribone et al. [16] stated that the normalized heat capacity curves with nearly equal height were fit to the TNM model better or worse depending on the absolute departure from equilibrium, in other words, depending on the annealing time and annealing temperature. The model became less accurate as annealing time increased or the annealing temperature increased, i.e. the departure from equilibrium became smaller.

The effect of the cooling–heating rate and aging or annealing time on the fitting parameters has been shown in several experiments [22,83,84] but the underling reasons are not clearly understood. The slight reduction in β with increasing temperature was also found in aging of sucrose [65], even though the TNM model explicitly assumes that β was independent of temperature by the assumption of thermorehological simplicity. The breakdown of the model has been assumed to be caused by the inappropriate partitioning of the structure and temperature dependence and/or by the inaccurate representation of the KWW relaxation function for the underlying physical mechanisms involved in the enthalpy relaxation process. However, O'Reilly and Hodge [81] noted that the failure of the TNM model likely lied in the handling of the non-linearity since the KWW stretched exponential function was known to give a good fit to linear relaxation data near structural equilibrium. The failure is either because of the incorrect form of $\tau(T, T_f)$ or the use of the reduced time ζ (Eq. (1)) to linearize the data in the TNM and Adam–Gibbs models.

5. Conclusions

The dynamics of enthalpy relaxation near the glass transition of glucose–fructose systems have been studied using differential scanning calorimetry. The evaluation of the relaxation parameters using the curve-fitting method showed similar results for both the TNM and Adam–Gibbs models. The higher values of parameter x for fructose compare to glucose indicate that the temperature dependence of the relaxation time increased as the amount of fructose content increased in the system. On the other hand, the lower values of β for fructose show that it has a broader relaxation time distribution spectrum compared to glucose. The decomposition of fructose during melting and its small relaxation above T_g was suspected to cause the lower value of activation energy Δh^* compared to that found by other researchers. Ignoring the thermal lag and the use of the function $f(x)$ instead of $F(x)$ may have produced the higher value of parameter x for the peak-shift method compared to the curve-fitting method for the TNM and Adam–Gibbs models. The relaxation behavior of the sugar systems was found to correlate to the "strong/fragile" classification. The stronger sugar (fructose) exhibits less non-Arrhenius behavior and possesses a higher value of x and the more fragile sugar (glucose) exhibits more non-linear behavior and possesses a lower value of parameter x. However, the empirical Eq. (20) was not found to adequately predict the relationship between the fragility index and the non-linearity parameter x in the sugar systems studied. Another expression may be needed.

Acknowledgements

I would like to respectfully acknowledge the assistance of Professor Thomas L. Jackson, Department of Computational Science and Engineering, University of Illinois at Urbana-Champaign, for his guidance in the computer modeling aspect of this research.

References

[1] C.T. Moynihan, S.N. Crichton, S.M. Opalka, J. Non-Cryst. Solids 131/133 (1991) 420–434.

[2] M.A. Debotl, A.J. Easteal, P.B. Macedo, C.T. Moynihan, J. Am. Ceram. Soc. 59 (1976) 16–21.
[3] S. Brawer, Relaxation in Viscous Liquids and Glasses: Review of Phenomenology, Molecular Dynamics Simulations, and Theoretical Treatment, The American Ceramic Society, Columbus, OH, 1985, pp. 1–3.
[4] A.J. Kovacs, J.M. Hutchinson, J.J. Aklonis, in: P.H. Gaskell (Ed.), The Structure of Non-Crystalline Materials, Taylor & Francis, London, 1977.
[5] L.C.E. Struik, Physical Aging of Amorphous Polymers and Other Materials, Elsevier, New York, 1978.
[6] Y. Roos, Phase Transitions in Foods, Academic Press, San Diego, CA, 1995.
[7] A.J. Kovacs, A.R. Stratton, J.D. Ferry, J. Chem. Phys. 67 (1963) 152.
[8] A.R. Berens, I.M. Hodge, Macromolecules 15 (1982) 756.
[9] I.M. Hodge, Macromolecules 20 (1987) 2897–2908.
[10] I.M. Hodge, J. Non-Cryst. Solids 131/133 (1991) 435–441.
[11] I.M. Hodge, J. Non-Cryst. Solids 169 (1994) 211–266.
[12] S.J. Schmidt, A.M. Lammert, J. Food Sci. 61 (1996) 870–875.
[13] R. Urbani, F. Sussich, S. Prejac, A. Cesaro, Themochim. Acta 304/305 (1997) 356–367.
[14] A.M. Lammert, S.J. Schmidt, J. Thermal Anal. 55 (1999) 949–975.
[15] C.A. Angell, Strong and fragile liquids, in: K. Ngai, G.B Wright (Eds.), Relaxation in Complex Systems, National Technical Information Services, US Department of Commerce, Springfield, VA, 1985.
[16] J.J. Tribone, J.M. O'Reilly, J. Greener, Macromolecules 19 (1986) 1732–1739.
[17] O.S. Narayanaswamy, J. Am. Ceram. Soc. 54 (1971) 491–498.
[18] R. Gardon, O.S. Narayanaswamy, J. Am. Ceram. Soc. 53 (1970) 380–385.
[19] A.Q. Tool, J. Am. Ceram. Soc. 29 (1946) 240–253.
[20] C.T. Moynihan, A.J. Easteal, M.A. DeBolt, J. Tucker, J. Am. Ceramic Soc. 59 (1976) 12–16.
[21] G.W. Scherer, J. Am. Ceram. Soc. 69 (1986) 374–381.
[22] G.W. Scherer, J. Am. Ceram. Soc. 67 (1984) 504.
[23] I.M. Hodge, Macromolecules 19 (1986) 936–938.
[24] A.J. Kovacs, J.M. Hutchinson, J. Polym. Sci.: Polym. Phys. Ed. 17 (1979) 2031–2058.
[25] J.M. Hutchinson, Polym. Int. 47 (1998) 56–64.
[26] J.M. Hutchinson, M. Ruddy, J. Polym. Sci.: Polym. Phys. Ed. 26 (1988) 2341–2366.
[27] J.M. Hutchinson, Thermal cycling of glasses: a theoretical and experimental approach, in: Th. Dorfrmiller, G. Williams (Eds.), Lecture Notes in Physics: Molecular Dynamics and Relaxation Phenomena in Glasses, Vol. 277, Springer, Berlin, 1987, pp. 172–187.
[28] A.R. Ramos, J.M. Hutchinson, A.J. Kovacs, J. Polym. Sci.: Polym. Phys. Ed. 22 (1984) 1655–1695.
[29] J.M. Hutchinson, A.J. Kovacs, Polym. Eng. Sci. 24 (1984) 1087–1103.
[30] P. Cortes, S. Montserrat, J. Polym. Sci.: Polm. Phys. Ed. 36 (1998) 113–116.
[31] P. Cortes, S. Montserrat, J. Ledru, J.M. Saiter, J. Non-Cryst. Solids 235/237 (1998) 522–526.
[32] S. Montserrat, J.L. Gomez Ribelles, J.M. Messeguer, Polymer 39 (1998) 3801–3807.
[33] P. Cortes, S. Montserrat, J.M. Hutchinson, J. Appl. Polym. Sci. 63 (1997) 17–25.
[34] J.M. Hutchison, D. McCarthy, S. Montserrat, P. Cortes, J. Polym. Sci.: Polym. Phys. Ed. 34 (1996) 229–231.
[35] S. Montserrat, P. Cortes, A.J. Pappin, K.H. Quah, J.M. Hutchinson, J. Non-Cryst. Solids 172/174 (1994) 1017–1022.
[36] A.J. Peppin, J.M. Hutchinson, M.D. Ingram, J. Non-Cryst. Solids 172/174 (1994) 584–591.
[37] A.J. Peppin, J.M. Hutchinson, M.D. Ingram, Macromolecules 25 (1992) 1084–1089.
[38] M.D. Ingram, J.M. Hutchinson, A.J. Pappin, Chem. Glasses 32 (1991) 121–128.
[39] C.A. Angell, J. Phys. Chem. Solids 49 (1988) 863–871.
[40] C.A. Angell, J. Non-Cryst. Solids 131/133 (1991) 13–31.
[41] C.A. Angell, Science 267 (1995) 1924–1935.
[42] C.A. Angell, Polymer 38 (1997) 6261–6266.
[43] C.A. Angell, L. Monnerie, L.M. Torell, Mater. Res. Soc. Symp. Proc. 215 (1991) 3–9.
[44] C.A. Angell, R.D. Bressel, J.L. Green, H. Kanno, M. Oguni, E.J. Sare, J. Food Eng. 22 (1994) 115–142.
[45] C.A. Angell, R.D. Bressel, J.L. Green, H. Kanno, M. Oguni, E.J. Sare, Liquid fragility and the glass transition in water and aqueous solutions, in: P. Fito, A. Mulet, B. Mc Kenna (Eds.), Water in Foods, Elsevier, London, 1994, pp. 115–142.
[46] B.C. Sales, J. Non-Cryst. Solids 119 (1990) 136–150.
[47] T.A. Vilgis, Phys. Rev. B 47 (1993) 2882–2885.
[48] R. Bohmer, Non-Cryst. Solids 172/174 (1994) 628–634.
[49] J.M. Hutchinson, M.D. Ingram, A.J. Pappin, J. Non-Cryst. Solids 131/133 (1991) 483–487.
[50] M. Godard, J. Saiter, J. Non-Cryst. Solids 235/237 (1998) 635–639.
[51] TA Instruments, Thermal Solutions: Heat Capacity Analysis Manual, PN 925635.002, Rev. B, New Castle, DE, 1997.
[52] TA Instruments, Universal Analysis Operator's Manual, PN 925609.002, New Castle, DE, 1996.
[53] M. Godard, J. Saiter, F. Burel, C. Bunel, P. Cortes, S. Montserrat, J.M. Hutchinson, Polym. Eng. Sci. 36 (1996) 2978–2985.
[54] R.R. Lagasse, J. Polym. Sci.: Polym. Phys. Ed. 20 (1982) 279–295.
[55] J.M.G. Cowie, R. Ferguson, Polymer 34 (1993) 2134–2141.
[56] I.M. Hodge, A.R. Berens, Macromolecules 15 (1982) 762–770.
[57] R. Wungtanagorn, Ph.D. Thesis, University of Illinois, Urbana-Champaign, 2000.
[58] M.J. Richardson, N.G. Savill, Polymer 16 (1975) 753–757.
[59] D. Simatos, G. Blond, G. Roudaut, D. Champion, J. Perez, J.A.L. Faivre, J. Thermal Anal. 47 (1996) 1419–1436.
[60] L. Finegold, F. Franks, R.H.M. Hatle, J. Chem. Soc., Faraday Trans. 85 (1989) 2445–2451.
[61] F. Frank, Pure Appl. Chem. 59 (1987) 1189–1202.
[62] C.A. Angell, F. Fan, Thermochim. Acta 266 (1995) 9–30.
[63] I.M. Hodge, G.S. Huvard, Macromolecules 16 (1983) 371–375.

[64] B.C. Handcock, S.L. Shamblin, G. Zografi, Pharm. Res. 12 (1995) 799–806.
[65] I.M. Hodge, Macromolecules 16 (1983) 898–902.
[66] J. Huang, P.K. Gupta, J. Non-Cryst. Solids 139 (1992) 239–247.
[67] I.M. Hodge, Science 267 (1995) 1945–1947.
[68] A.J. Kovacs, J.J. Aklonis, J.M. Hutchinson, A.R. Ramos, J. Polym. Sci.: Polym. Phys. Ed. 17 (1979) 1097–1162.
[69] J. Malek, Thermochim. Acta 313 (1998) 181–190.
[70] J. Malek, S. Montserrat, Thermochim. Acta 313 (1998) 191–200.
[71] J.M. Hutchinson, M. Ruddy, M.R. Wilson, Polymer 29 (1988) 152–159.
[72] M. Tatsumisago, C.A. Angell, J. Chem. Phys. 92 (1989) 617.
[73] R. Bohmer, K.L. Ngai, C.A. Angell, D.J. Plazek, J. Chem. Phys. 5 (1993) 4201–4209.
[74] D. Simatos, G. Blond, J. Perez, Basic physical aspects of glass transition, in: G.V. Barbosa-Canovas, J. Welti-Chanes (Eds.), Food Preservation by Moisture Control: Fundamentals and Applications, Thecnomic Publishing Company, Lancaster, PA, 1995.
[75] C.T. Moynihan, J. Schroeder, J. Non-Cryst. Solids 160 (1993) 52–59.
[76] A.L. Ollett, R. Parker, J. Texture Stud. 21 (1990) 355–362.
[77] J. Perez, J.Y. Cavaille, J. Non-Cryst. Solids 172/174 (1994) 1028–1036.
[78] C.A. Angell, D.L. Smith, J. Phys. Chem. 86 (1982) 3845–3852.
[79] A. Brunacci, J.M.G. Cowie, R. Ferguson, J.L. Gomez Ribelles, A. Vidaurre Garayo, Macromolecules 29 (1996) 7976–7988.
[80] J.M. O'Reilly, I.M. Hodge, J. Non-Cryst. Solids 131/133 (1991) 451–456.
[81] Y. Han, A. D'Amore, G. Marino, L. Nicolais, Mater. Chem. Phys. 55 (1998) 155–159.
[82] S. Matsuoka, G.H. Fredrickson, G.E. Johnson, Application of Adam–Gibbs' theory to thermodynamic recovery and structural relaxation, in: Th. Dorfrmiller, G. Williams (Eds.), Lecture Notes in Physics: Molecular Dynamics and Relaxation Phenomena in Glasses, Vol. 277, Springer, Berlin, 1987, pp. 188–202.
[83] C.T. Moynihan, S.M. Opalka, R. Mossadegh, S. N. Crichton, A.J. Bruce, Sub-T_g relaxation in heavy metal fluoride glasses, in: Th. Dorfrmiller, G. Williams (Eds.), Lecture Notes in Physics: Molecular Dynamics and Relaxation Phenomena in Glasses, Vol. 277, Springer, Berlin, 1987, pp. 16–26.
[84] W. Pascheto, M.G. Parthun, A. Hallbrucker, G.P. Johari, J. Non-Cryst. Solids 171 (1994) 182–190.